

Vortex loop dynamics and dynamical quantum phase transitions in three-dimensional fermion matter

Arkadiusz Kosior, Markus Heyl

Angaben zur Veröffentlichung / Publication details:

Kosior, Arkadiusz, and Markus Heyl. 2024. "Vortex loop dynamics and dynamical quantum phase transitions in three-dimensional fermion matter." *Physical Review B* 109 (14): L140303. <https://doi.org/10.1103/physrevb.109.1140303>.

Nutzungsbedingungen / Terms of use:

licgercopyright

Dieses Dokument wird unter folgenden Bedingungen zur Verfügung gestellt: / This document is made available under these conditions:

Deutsches Urheberrecht

Weitere Informationen finden Sie unter: / For more information see:

<https://www.uni-augsburg.de/de/organisation/bibliothek/publizieren-zitieren-archivieren/publiz/>



Vortex loop dynamics and dynamical quantum phase transitions in three-dimensional fermion matter

Arkadiusz Kosior¹ and Markus Heyl^{2,3}

¹*Institute for Theoretical Physics, University of Innsbruck, 6020 Innsbruck, Austria*

²*Theoretical Physics III, Center for Electronic Correlations and Magnetism, Institute of Physics, University of Augsburg, 86135 Augsburg, Germany*

³*Max-Planck-Institut für Physik Komplexer Systeme, Nöthnitzer Strasse 38, D-01187 Dresden, Germany*



(Received 27 July 2023; revised 28 February 2024; accepted 12 March 2024; published 15 April 2024)

Over the past decade, dynamical quantum phase transitions (DQPTs) have emerged as a paradigm shift in understanding nonequilibrium quantum many-body systems. However, the challenge lies in identifying order parameters that effectively characterize the associated dynamic phases. In this study we investigate the behavior of vortex singularities in the phase of the Green's function for a broad class of fermion lattice models in three dimensions after an instantaneous quench in both interacting and noninteracting systems. We find that the full set of vortices form one-dimensional dynamical objects, which we call *vortex loops*. We propose that the number of such vortex loops can be interpreted as a quantized order parameter that distinguishes between different nonequilibrium phases. Our results establish an explicit link between variations in the order parameter and DQPTs in the noninteracting scenario. Moreover, we show that the vortex loops are robust in the weakly interacting case, even though there is no direct relation between the Loschmidt amplitude and the Green's function. Finally, we observe that vortex loops can form complex dynamical patterns in momentum space. Our findings provide valuable insights for developing definitions of dynamical order parameters in nonequilibrium systems.

DOI: [10.1103/PhysRevB.109.L140303](https://doi.org/10.1103/PhysRevB.109.L140303)

Introduction. Due to advancements in experimental technologies and a deeper theoretical understanding, the field of nonequilibrium quantum many-body dynamics has rapidly progressed in the last ten years [1]. This has led to the exploration of exciting, ergodicity-broken states and phases of quantum matter [2,3], such as many-body scars [4] and time crystals [5,6], which are of inherent nonequilibrium nature and go beyond standard thermodynamics and the theory of quantum phase transitions [7,8]. It has also been discovered that a nonequilibrium unitary evolution of quantum states can give rise to temporal nonanalyticities in the rate of the Loschmidt amplitude, which is analogous to the singularities observed in thermodynamic functions during equilibrium phase transitions. This phenomenon, termed a dynamical quantum phase transition (DQPT) [9–12], has recently attracted a lot of attention from both the theoretical [13–33] and experimental [34–38] communities (for related nonequilibrium transitions characterized by order parameters, see Refs. [39–42]). While it has been demonstrated in different cases that DQPTs are directly linked to the equilibrium phase transition of the system being studied, this connection cannot be considered a one-to-one correspondence in general [43]. Therefore, DQPT is expected to be a genuine nonequilibrium phenomenon without an equilibrium counterpart, requiring the identification of order parameters that precisely characterize the dynamic phases in question. Remarkably, DQPTs for a noninteracting system in two dimensions (2D) can be closely related to the emergence of measurable, dynamic vortexlike singularities in the phase of the Green's function in

momentum space [44–47] (for experiments see [34,48]). It has been shown so far that the vortices appear as stable objects in 2D two-band models, but higher-dimensional systems have remained unexplored so far.

In the following we demonstrate that in a broad class of three-dimensional (3D) lattice models, with both interacting and noninteracting fermions, the vortices of the Green's function are not isolated; instead, they form one-dimensional (1D) dynamical *vortex loops*. We argue that the number of these vortex loops can be interpreted as a quantized order parameter that distinguishes between different nonequilibrium phases. Although focusing on a simple Weyl semimetal model with two bands [49–54], we provide arguments and examples that our results are applicable to a wide class of fermionic, translationally symmetric lattice models in 3D [55]. Importantly, we show that the vortex loops are robust and survive in weakly interacting systems, even though there is no direct relation between the Loschmidt amplitude and the Green's function. Additionally, due to the existence of band-touching Weyl nodes, we find that in a long time limit the loops can form complex dynamical patterns in momentum space.

General setup and observables. Before we turn to a specific microscopic model, we start this section with a very general picture. We consider a particle-hole symmetric model of noninteracting spin-1/2 fermions with translational invariance on a 3D lattice. The Hamiltonian of such a system can be written in the form

$$\hat{H} = \sum_{\mathbf{k} \in \text{BZ}} \hat{\psi}_{\mathbf{k}}^{\dagger} H_{\mathbf{k}} \hat{\psi}_{\mathbf{k}}, \quad H_{\mathbf{k}} = \vec{h}_{\mathbf{k}} \cdot \vec{\sigma}, \quad (1)$$

with the summation going over independent quasimomenta \mathbf{k} of a Brillouin zone (BZ). Here $\hat{\psi}_{\mathbf{k}}$ denotes a fermionic spinor operator, $\vec{\sigma}$ is a vector of Pauli matrices, and $\vec{h}_{\mathbf{k}}$ is a vector defined by microscopic details of a particular model. Here, without a loss of generality, we consider $\hat{\psi}_{\mathbf{k}}^{\dagger} = [\hat{c}_{\mathbf{k},\uparrow}^{\dagger}, \hat{c}_{\mathbf{k},\downarrow}^{\dagger}]$ with $\hat{c}_{\mathbf{k},\sigma=\uparrow,\downarrow}^{\dagger}$ being standard creation operators [56], but we note that the precise form of $\hat{\psi}_{\mathbf{k}}$ might also be different depending on the choice of a two-band model. Throughout this work we adopt a unit lattice spacing and set $\hbar = 1$.

Furthermore, we assume that the system is prepared in a fermionic ground state at a half filling, namely, $|\psi_0\rangle = \Pi_{\mathbf{k}\in\text{BZ}}|\mathbf{k}_{-}^{(i)}\rangle$, where $|\mathbf{k}_{-}^{(i)}\rangle = \hat{c}_{\mathbf{k}}^{(i)\dagger}|0\rangle$ is the lower state of some initial Hamiltonian $H_{\mathbf{k}}^{(i)} = \vec{h}_{\mathbf{k}}^{(i)} \cdot \vec{\sigma}$, see [57]. At a time $t = 0$ we perform an instantaneous quench of at least one of the model's parameters, which results in a sudden change of the Hamiltonian $\vec{h}_{\mathbf{k}}^{(i)} \rightarrow \vec{h}_{\mathbf{k}}^{(f)}$. After the quench, the initial state $|\psi_0\rangle$ evolves under the new Hamiltonian $H_{\mathbf{k}}^{(f)} = \vec{h}_{\mathbf{k}}^{(f)} \cdot \vec{\sigma}$, i.e., $|\psi(t)\rangle = \Pi_{\mathbf{k}\in\text{BZ}}|\mathbf{k}(t)\rangle$, with

$$|\mathbf{k}(t)\rangle = \sum_{\alpha=\pm} \Gamma_{\mathbf{k}}^{\alpha} e^{-i\epsilon_{\mathbf{k},\alpha}t} |\mathbf{k}_{\alpha}^{(f)}\rangle, \quad \Gamma_{\mathbf{k}}^{\alpha} = \langle \mathbf{k}_{\alpha}^{(f)} | \mathbf{k}_{-}^{(i)} \rangle, \quad (2)$$

where $|\mathbf{k}_{\alpha}^{(f)}\rangle = \hat{c}_{\mathbf{k},\alpha}^{(f)\dagger}|0\rangle$ is an eigenvector of $H_{\mathbf{k}}^{(f)}$ with the corresponding eigenenergy $\epsilon_{\mathbf{k},\alpha=\pm} = \pm\epsilon_{\mathbf{k}}$. We assume that the quench preserves translational invariance so that a quasimomentum \mathbf{k} remains a good quantum number.

To investigate the dynamics of the nonequilibrium system, we focus on the time-ordered Green's function [58],

$$g_{\mathbf{k}}(t) = \sum_{\mathbf{r},\sigma} e^{i\mathbf{k}\cdot\mathbf{r}} \langle \hat{c}_{\mathbf{r},\sigma}(t)^{\dagger} \hat{c}_{\mathbf{r}=0,\sigma} \rangle = \sum_{\mathbf{q},\sigma} \langle \hat{c}_{\mathbf{k},\sigma}^{\dagger}(t) \hat{c}_{\mathbf{q},\sigma} \rangle, \quad (3)$$

where in the above we denote $\langle \dots \rangle = \langle \psi_0 | \dots | \psi_0 \rangle$ and $\hat{c}_{\mathbf{r},\sigma} = 1/\sqrt{N} \sum_{\mathbf{k}} e^{-i\mathbf{k}\cdot\mathbf{r}} \hat{c}_{\mathbf{k},\sigma}$. Alternatively, one could also study the Loschmidt amplitude $\mathcal{G}(t) = \langle \psi_0 | \psi(t) \rangle = \langle \psi_0 | e^{-iH^{(f)}t} | \psi_0 \rangle$, which quantifies how far the time evolution drives the system away from the initial condition. The Loschmidt amplitude can be conveniently written as $\mathcal{G}(t) = \Pi_{\mathbf{k}} \mathcal{G}_{\mathbf{k}}^{(1)}(t)$, with

$$\mathcal{G}_{\mathbf{k}}^{(1)}(t) = \langle 0 | \hat{c}_{\mathbf{k}}^{(i)\dagger}(t) \hat{c}_{\mathbf{k}}^{(i)} | 0 \rangle = \langle \mathbf{k}_{-}^{(i)} | \mathbf{k}(t) \rangle. \quad (4)$$

Since the Loschmidt amplitude \mathcal{G} for a many-body system is a fast-decaying function with the increasing number of particles N , it is convenient to define the rate function, $\lambda = -\lim_{N \rightarrow \infty} \ln |\mathcal{G}|^2 / N$. The latter bears formal resemblance to the free-energy density (with temperature replaced by time t) and, therefore, λ might be viewed as a nonequilibrium free-energy analog. This analogy implies that the rate function λ can show signatures of a phase transition having non-analytic points that appear dynamically in time giving rise to a *dynamical quantum phase transition* (DQPT) [9–12]. For the considered setup the rate function can be expressed analytically, i.e.,

$$\lambda(t) = - \int \frac{d\mathbf{k}}{(2\pi)^3} \ln [1 + [(\hat{h}_{\mathbf{k}}^{(i)} \cdot \hat{h}_{\mathbf{k}}^{(f)})^2 - 1] \sin^2(\epsilon_{\mathbf{k}}t)], \quad (5)$$

with the normalized vectors $\hat{h}_{\mathbf{k}} = \vec{h}_{\mathbf{k}} / (\vec{h}_{\mathbf{k}} \cdot \vec{h}_{\mathbf{k}})^{1/2}$.

To ensure clarity, throughout this Letter we have chosen to focus on a single model while still drawing general conclusions [55]. Specifically, we consider a two-band 3D Weyl

semimetal Hamiltonian [59], given by

$$\vec{h}_{\mathbf{k}} = [\sin k_x, \sin k_y, m_z - \cos k_z], \quad (6)$$

and we assume a quench of the free parameter m_z between two distinct topological phases: a normal insulator ($|m_z| > 1$) and a Weyl semimetal ($|m_z| < 1$) characterized by pairs of Weyl points and linear Dirac-like dispersion around them. As we will demonstrate, this quench induces a DQPT and leads to the appearance of 1D dynamical singularities in the phase of the Green's function.

Relating DQPTs with phase singularities. For a noninteracting system, it can be shown that $\mathcal{G}_{\mathbf{k}}^{(1)} = \overline{g_{\mathbf{k}}}$, i.e., the Green's function is a complex conjugate of the first-order correlation function [60], which implies that a DQPT can be observed on a Green's-function level. Indeed, the nonanalytic points of the rate function $\lambda(t)$ can only occur if and only if $g_{\mathbf{k}}(t) = |g_{\mathbf{k}}(t)| \exp[i\phi_{\mathbf{k}}(t)]$ vanishes for some \mathbf{k}^* and t^* , implying a phase singularity of the Green's function $\phi_{\mathbf{k}}(t)$ [11]. While in 1D systems the phase singularities can be only observed in a $k-t$ plane [13,61], in 2D models these singularities appear as isolated dynamical point vortices with clockwise or anticlockwise phase winding [44–47] (for experiments see Refs. [34,48]). On the other hand, in the following sections we argue that for a wide class of 3D models these vortices group together, forming dynamical 1D objects, i.e., *vortex loops*, which can be either contractible or incontractible. The number of these objects can be associated with dynamical order parameters which identify different nonequilibrium phases. In turn, a change of a dynamical order parameter is accompanied by a DQPT, i.e., a temporal singularity of the rate function λ . Later in this Letter we show that the vortex loops also appear in interacting systems, although there is no strict relation between the Green's function $g_{\mathbf{k}}$ and the Loschmidt amplitude \mathcal{G} anymore.

Dynamics of vortex loops. For a generic, noninteracting two-band model, a complex valued condition $g_{\mathbf{k}}(t) = \sum_{\alpha} |\Gamma_{\mathbf{k}}^{\alpha}|^2 e^{i\epsilon_{\mathbf{k},\alpha}t} = 0$ implies

$$(i) \mathcal{M} : |\Gamma_{\mathbf{k}}^{\pm}|^2 = \frac{1}{2}, \quad (ii) \mathcal{M}_n(t) : t_n = \frac{(2n+1)\pi}{2\epsilon_{\mathbf{k}}}, \quad (7)$$

with $n \in \mathbb{N}$, $\epsilon_{\mathbf{k},\alpha=\pm} = \pm\epsilon_{\mathbf{k}}$ and $\Gamma_{\mathbf{k}}^{\alpha}$ defined as in Eq. (2). In 3D, the conditions in Eq. (7) define two 2D surfaces in the momentum space. The first condition defines a static manifold, \mathcal{M} , illustrated as the orange surface in Fig. 1. The second condition defines a dynamical, equienergy surface, $\mathcal{M}_n(t)$, that can intersect with \mathcal{M} during some time intervals. Here we assume that \mathcal{M} and $\mathcal{M}_n(t)$ are smooth 2D surfaces within the 3D Brillouin zone [62]. The 3D Brillouin zone, being a 3-torus, is a compact manifold with no boundary, i.e., it is a closed manifold. Consequently, also \mathcal{M} , $\mathcal{M}_n(t)$ and their nonempty intersection are also closed and smooth, consisting of closed curves (i.e., the vortex loops) and/or isolated points when the vortex loops are being created or annihilated [63].

The vortex loops in different stages of evolution are illustrated in Fig. 1 by the blue and red curves. For our analysis, we have selected a 3D Weyl Hamiltonian [59], determined by Eq. (6), with $m_z^{(i)} = 2.5$ and $m_z^{(f)} = 0$. In this case, \mathcal{M} is a connected surface with a nonzero genus [64] and, therefore, any closed curve on this surface can be classified as either

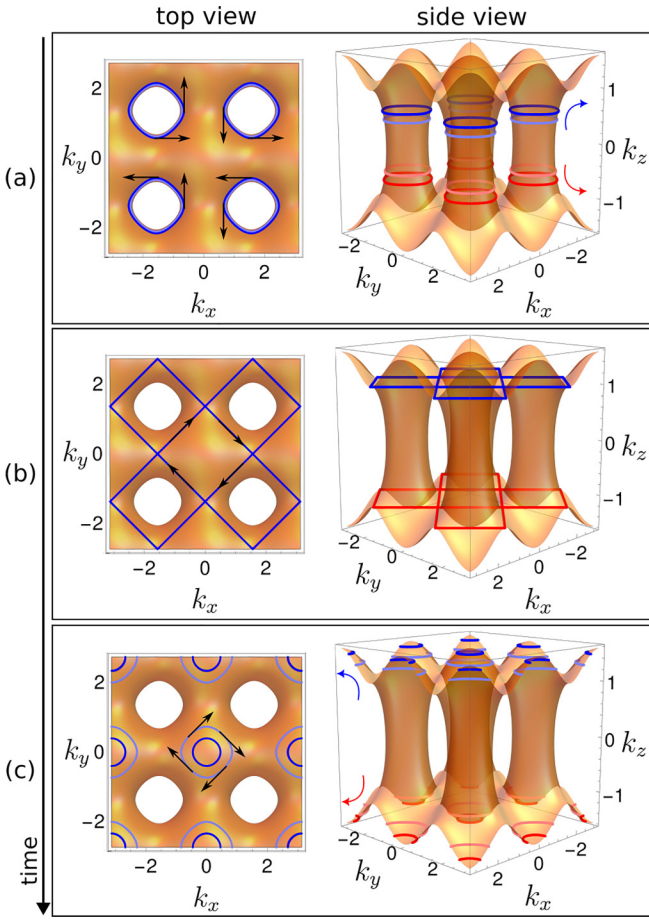


FIG. 1. Exemplary dynamics of vortex loops on a static manifold \mathcal{M} (orange surface) in a 3D BZ. The red and blue colors represent the chirality of the loops. (a) Incontractible loop with opposing chiralities are created in pairs and move in opposite directions; light colors correspond to $t = 1.05$ and dark colors to $t = 1.1$. (b) Loops of the same chirality can merge if their tangent vectors (black arrows) are antiparallel at the loops' touching points; $t = 1.405$ (c) Through loop merging, the loops can change their topological character from incontractible to contractible loops; $t = 2$ (light colors), $t = 3.5$ (dark colors).

a contractible or incontractible loop. Further examples of \mathcal{M} can be found in the Supplemental Material [55].

In addition, the loops can also be characterized based on their chirality, indicated by \pm , see Fig. 2(a). Specifically, any closed curve circulating a vortex loop undergoes a phase jump of $\Delta\phi = \pm 2\pi$, where the sign of the jump represents the chirality of the loop. Loop chiralities are important in terms of their dynamics, e.g., loop merging or loop creation as explained in the following.

In a typical scenario, the vortex loops are created at certain times, $t_n^{(c)} = (2n + 1)\pi / (2\epsilon_{\max})$, and annihilated at $t_n^{(a)} = (2n + 1)\pi / (2\epsilon_{\min})$, $n \in \mathbb{N}$, where ϵ_{\max} (ϵ_{\min}) is the maximal (minimal) value of the upper band dispersion relation over quasimomenta \mathbf{k} belonging to \mathcal{M} , i.e., $\epsilon_{\max} = \max_{\mathbf{k} \in \mathcal{M}} \epsilon_{\mathbf{k}}$ ($\epsilon_{\min} = \min_{\mathbf{k} \in \mathcal{M}} \epsilon_{\mathbf{k}}$). As we show in Fig. 1(a), the loops can be created (or annihilated) in pairs with opposing chiralities, represented by red and blue colors. Alternatively, contractible loops can be also created from a single point of the BZ

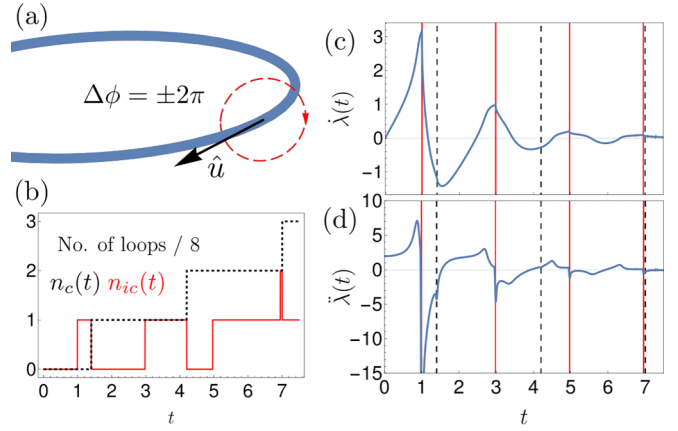


FIG. 2. (a) Chirality (\pm) of a vortex loop is determined by $\Delta\phi = \pm 2\pi$ phase jump while encircling a loop around a tangent vector \hat{u} . (b) The number of contractible $n_c(t)$ and incontractible $n_{ic}(t)$ loops can be considered as quantized dynamical order parameters (black dashed and red solid lines, respectively). (c), (d) The first and second derivative of the rate function $\lambda(t)$ with nonanalytic DQPT points (marked by vertical lines) exactly match the changes of $n_c(t)$ and $n_{ic}(t)$.

and annihilated in the inverse process. In the course of time evolution, the vortex loops of the same chirality can merge together, as long as their tangent vectors at the touching point are antiparallel, for example, see Fig. 1(b). Through the loop merging, it is even possible that the loops change their topological character from incontractible to contractible [see Fig. 1(c)], or vice versa.

The dynamics of vortex loops is rather complex but can be captured qualitatively and quantitatively by monitoring the number of loops over time, denoted as $n_c(t)$ and $n_{ic}(t)$ for contractible and incontractible loops, respectively [Fig. 2(b)]. These numbers of vortices can be interpreted as quantized dynamical order parameters that distinguish between different nonequilibrium phases. To support this interpretation, we plot the first and second derivative of the rate function $\lambda(t)$, given by Eq. (5), in Figs. 2(c) and 2(d). In this work we study a parameter quench from a normal insulator phase to a Weyl semimetal phase [59], which passes through a critical point of an equilibrium quantum phase transition, resulting in a change in the topological properties of the underlying Hamiltonian. Our analysis reveals a sequence of nonanalytic points in time, which corresponds to a series of DQPT events, as per the definition [11]. Within our model, we observe two types of nonanalytic points: those corresponding to a discontinuity in the second derivative of $\lambda(t)$ and those corresponding to a divergence of $\ddot{\lambda}(t)$. By comparing the critical times with the number of vortex loops of each kind, we observe that the appearance of each nonanalytic point is necessarily associated with a change in $n_c(t)$ or $n_{ic}(t)$.

Effects of interactions. So far we have focused on a noninteracting fermionic model. In this section we aim to demonstrate that our findings are more general and robust by showing that the vortex loops persist even in the presence of weak interactions. Consequently, let us consider $H = H_0 + \eta V$, with η being a small interaction strength and V being a generic two-body interaction term. To calculate the Green's

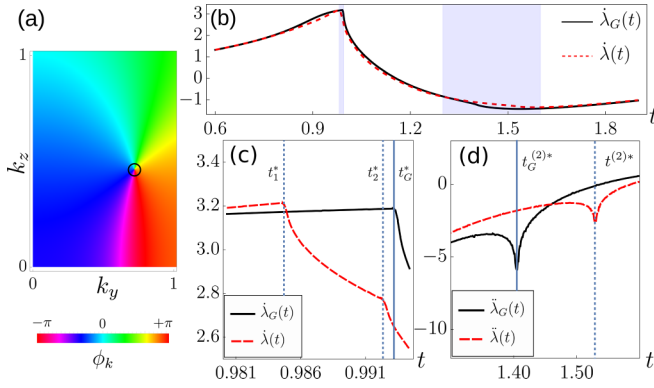


FIG. 3. (a) The phase of the Green's function $g_{\mathbf{k}}(t)$ in the interacting regime is shown for interaction strength $\eta = 0.1$ and time $t = 1.05$ with a fixed value of $k_x = \pi/2$. The black circle marks the position of the vortex in the noninteracting case. (b) The first derivatives of the rate function $\lambda(t)$ (red dashed line) and $\lambda_G(t)$ (black solid), the latter being defined in Eq. (10). Although the two curves almost overlap, their nonanalytic points do not coincide and their mismatch grows in time. Nonanalytic points of $\lambda(t)$ and $\lambda_G(t)$ are contained within the two shaded areas, as depicted in panels (c) and (d), respectively. (c) Zoom-in of $\lambda(t)$ and $\lambda_G(t)$ in a vicinity of the first temporal nonanalytic points at t_1^* , t_2^* , and t_G^* . (d) Zoom-in of $\lambda(t)$ and $\lambda_G(t)$ showing the second type of nonanalytic points at $t^{(2)*}$ and $t_G^{(2)*}$.

function $g_{\mathbf{k}}(t)$ in the interacting regime, the only difficulty lies in obtaining the time evolution operator in the interaction picture $U(t)$. However, up to linear order in η , we can utilize the Magnus expansion [65,66] and truncate V to its leading terms [67] in order to approximate $U(t) \approx e^{-iH_0^t} \exp(-\Omega)$ with

$$\Omega(t) \approx -i\eta t \sum_{\mathbf{k}} \sum_{\alpha, \beta} \Lambda_{\mathbf{k}, \mathbf{k}'}^{\alpha, \beta} \hat{n}_{\mathbf{k}, \alpha}^{(t)} \hat{n}_{\mathbf{k}', \beta}^{(t)}, \quad (8)$$

where the coefficients $\Lambda_{\mathbf{k}, \mathbf{k}'}^{\alpha, \beta}$ depend on the specific interaction type. Here, we choose BCS interactions and get $\Lambda_{\mathbf{k}, \mathbf{k}'}^{\alpha, \beta} = \delta_{\mathbf{k}', -\mathbf{k}} |\gamma_{\mathbf{k}, \uparrow}^\alpha|^2 |\gamma_{\mathbf{k}', \downarrow}^\beta|^2$ with $\gamma_{\mathbf{k}, \sigma}^\alpha = \langle \mathbf{k}_\alpha^{(t)} | \mathbf{k}_\sigma \rangle$, see [68]. Inserting Eq. (8) into the formula for the Green's function, Eq. (3), one readily gets

$$g_{\mathbf{k}}(t) \approx \sum_{\alpha, \beta} |\Gamma_{\mathbf{k}, \alpha} \Gamma_{-\mathbf{k}, \beta}|^2 e^{it\epsilon_{\mathbf{k}, \alpha}} e^{-it(\Lambda_{\mathbf{k}, -\mathbf{k}}^{\alpha, \beta} + \Lambda_{\mathbf{k}, \mathbf{k}}^{\beta, \alpha})}, \quad (9)$$

with $\Gamma_{\mathbf{k}}^\alpha = \langle \mathbf{k}_\alpha^{(t)} | \mathbf{k}^{(i)} \rangle$. Following these steps, in Fig. 3(a) we plot the phase of $g_{\mathbf{k}}(t)$, choosing the interaction strength $\eta = 0.1$ and a time $t = 1.05$. For clarity of the presentation we fix $k_x = \pi/2$ and illustrate a 2D cut through momentum space, which shows a clear phase singularity close to the center of the panel. Although the interacting part of the Hamiltonian adds a correction to the Green's function, we find that within the numerical precision the position of the vortex in the momentum space matches the position of the vortex in the noninteracting case, marked by a black circle in Fig. 3(a).

As discussed, in the noninteracting system the vortex loop dynamics is inherently imprinted in the rate function $\lambda(t)$. In the following we explore whether this relation still holds for the interacting case. In Fig. 3(b) we illustrate the first

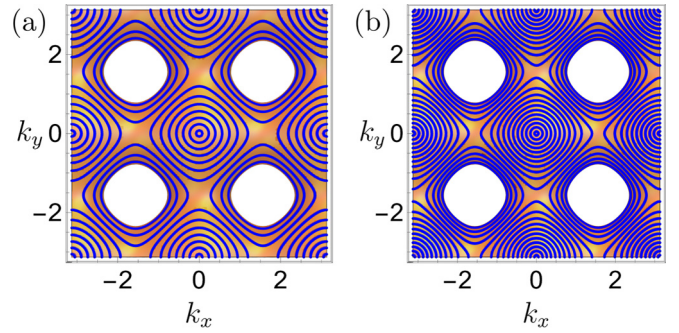


FIG. 4. The complex pattern formed by loop vortices at times $t = 15$ [panel (a)] and $t = 30$ [panel (b)] after the quench to the Weyl semimetal phase, where the number of loops around the Weyl nodes increases linearly in time. Due to the dispersion relation $\epsilon_{\mathbf{k}}$ vanishing for some points belonging to the manifold \mathcal{M} , the loops never annihilate and instead, their dynamics slows down, leading to their accumulation around the band touching points \mathbf{k}_W . The resulting dynamical pattern cannot be destroyed due to the system's dynamics.

derivative of the rate function $\lambda(t)$ (the red dashed line) in the vicinity of the first nonanalytic point in time, which for $\eta = 0.1$ is close to $t^* \approx 0.985$. In order to quantitatively determine the point in time associated with the loops' creation and directly compare the behavior of the Loschmidt amplitude and the Green's function, we define

$$\lambda_G(t) = - \lim_{N \rightarrow \infty} \ln |\Pi_{\mathbf{k}} g_{\mathbf{k}}(t)|^2 / N \quad (10)$$

and plot its first derivative in Fig. 3(b) (the black solid line). Although at first glance the first derivatives of $\lambda(t)$ and $\lambda_G(t)$ exhibit strikingly close overlap, it is noteworthy that their nonanalytic points do not coincide [Figs. 3(c) and 3(d)]. On the contrary, we find that the discrepancy between the nonanalytic points grows in time.

Dynamical pattern formation. Although the loop dynamics is rather complex, the loop creation and annihilation time can be determined easily from Eq. (7). In particular, the annihilation time is given by $t_n^{(a)} = (2n + 1)\pi / (2\epsilon_{\min})$, $n \in \mathbb{N}$, where $\epsilon_{\min} = \min_{\mathbf{k} \in \mathcal{M}} \epsilon_{\mathbf{k}}$. However, in our analysis presented in Fig. 2(b), the total number of loops never decreases in time due to the choice of the model and the quench to the Weyl semimetal phase, which hosts pairs of the band-touching Weyl nodes denoted by \mathbf{k}_W [59]. As the dispersion relation $\epsilon_{\mathbf{k}}$ vanishes for some points belonging to the manifold \mathcal{M} , the loops are never annihilated. Instead, the loops' dynamics slow down, and eventually, they accumulate around the band touching points \mathbf{k}_W . In Fig. 4 we show a complex pattern formed by the loop vortices at times $t = 15$ and $t = 30$ after the quench. Although the number of loops around the Weyl nodes increases linearly in time, the resulting dynamical pattern cannot be destroyed due to dynamics.

Summary and perspectives. The Green's function plays a crucial role in quantum many-body theory. Our main finding is that the Green's function in 3D fermion matter after a parameter quench involves the dynamical creation and annihilation of topological defects in momentum space in the form of vortex loops. We have demonstrated that these loops are triggered by an underlying dynamic quantum phase transi-

tion. As a consequence, these vortex loops act as a dynamic topological order parameter. Moreover, we have shown that the vortex loops survive in weakly interacting systems and that they can form complex dynamical patterns in momentum space due to the existence of band touch points.

Our findings reveal that nonequilibrium dynamics in 3D systems exhibit a significantly greater level of complexity compared to lower dimensions. As a result, it appears that to obtain a deeper understanding of the intricate out-of-equilibrium quantum phases of matter, there is a need to undertake further investigations on DQPTs specifically in 3D systems. We emphasize the importance of exploring further the connection between DQPT and vortex loops in interacting systems, especially beyond perturbative regimes. Such

exploration could potentially prompt a reevaluation of DQPT, shifting the focus from the Loschmidt amplitude to the involvement of the Green's function.

The data presented in this article is available from [69].

Acknowledgments. This research was funded in whole or in part by the Austrian Science Fund (FWF) [10.55776/ESP171]. This project has received funding from the European Research Council (ERC) under the European Union's Horizon 2020 Research and Innovation Program (Grant Agreement No. 853443). This work was supported by the German Research Foundation DFG via project 492547816 (TRR 360).

-
- [1] A. Polkovnikov, K. Sengupta, A. Silva, and M. Vengalattore, *Rev. Mod. Phys.* **83**, 863 (2011).
- [2] T. Mori, T. N. Ikeda, E. Kaminishi, and M. Ueda, *J. Phys. B: At. Mol. Opt. Phys.* **51**, 112001 (2018).
- [3] S. Moudgalya, B. A. Bernevig, and N. Regnault, *Rep. Prog. Phys.* **85**, 086501 (2022).
- [4] D. A. Abanin, E. Altman, I. Bloch, and M. Serbyn, *Rev. Mod. Phys.* **91**, 021001 (2019).
- [5] V. Khemani, R. Moessner, and S. L. Sondhi, [arXiv:1910.10745](https://arxiv.org/abs/1910.10745).
- [6] K. Sacha, *Time Crystals* (Springer International Publishing, Cham, Switzerland, 2020).
- [7] S. Sachdev, *Quantum Phase Transitions* (Cambridge University Press, Cambridge, England, 2000).
- [8] J. Dziarmaga, *Adv. Phys.* **59**, 1063 (2010).
- [9] M. Heyl, A. Polkovnikov, and S. Kehrein, *Phys. Rev. Lett.* **110**, 135704 (2013).
- [10] A. A. Zvyagin, *Low Temp. Phys.* **42**, 971 (2016).
- [11] M. Heyl, *Rep. Prog. Phys.* **81**, 054001 (2018).
- [12] M. Heyl, *Europhys. Lett.* **125**, 26001 (2019).
- [13] J. C. Budich and M. Heyl, *Phys. Rev. B* **93**, 085416 (2016).
- [14] J. C. Halimeh and V. Zauner-Stauber, *Phys. Rev. B* **96**, 134427 (2017).
- [15] B. Žunkovič, M. Heyl, M. Knap, and A. Silva, *Phys. Rev. Lett.* **120**, 130601 (2018).
- [16] J. Lang, B. Frank, and J. C. Halimeh, *Phys. Rev. Lett.* **121**, 130603 (2018).
- [17] M. Heyl, F. Pollmann, and B. Dóra, *Phys. Rev. Lett.* **121**, 016801 (2018).
- [18] A. Kosior and K. Sacha, *Phys. Rev. A* **97**, 053621 (2018).
- [19] A. Kosior, A. Syrwid, and K. Sacha, *Phys. Rev. A* **98**, 023612 (2018).
- [20] K. Yang, L. Zhou, W. Ma, X. Kong, P. Wang, X. Qin, X. Rong, Y. Wang, F. Shi, J. Gong *et al.*, *Phys. Rev. B* **100**, 085308 (2019).
- [21] L. Zhou and Q. Du, *New J. Phys.* **23**, 063041 (2021).
- [22] S. Peotta, F. Brange, A. Deger, T. Ojanen, and C. Flindt, *Phys. Rev. X* **11**, 041018 (2021).
- [23] D. Trapin, J. C. Halimeh, and M. Heyl, *Phys. Rev. B* **104**, 115159 (2021).
- [24] S. Bandyopadhyay, A. Polkovnikov, and A. Dutta, *Phys. Rev. Lett.* **126**, 200602 (2021).
- [25] J. C. Halimeh, D. Trapin, M. Van Damme, and M. Heyl, *Phys. Rev. B* **104**, 075130 (2021).
- [26] S. De Nicola, A. A. Michailidis, and M. Serbyn, *Phys. Rev. Lett.* **126**, 040602 (2021).
- [27] C. Y. Wong and W. C. Yu, *Phys. Rev. B* **105**, 174307 (2022).
- [28] J. Naji, R. Jafari, L. Zhou, and A. Langari, *Phys. Rev. B* **106**, 094314 (2022).
- [29] J. Naji, M. Jafari, R. Jafari, and A. Akbari, *Phys. Rev. A* **105**, 022220 (2022).
- [30] R. Jafari, A. Akbari, U. Mishra, and H. Johannesson, *Phys. Rev. B* **105**, 094311 (2022).
- [31] D. Mondal and T. Nag, *Phys. Rev. B* **107**, 184311 (2023).
- [32] K. Cao, H. Guo, and G. Yang, *J. Phys.: Condens. Matter* **36**, 155401 (2024).
- [33] C. Y. Wong, H. Cheraghi, and W. C. Yu, *Phys. Rev. B* **108**, 064305 (2023).
- [34] N. Fläschner, D. Vogel, M. Tarnowski, B. S. Rem, D.-S. Lühmann, M. Heyl, J. C. Budich, L. Mathey, K. Sengstock, and C. Weitenberg, *Nat. Phys.* **14**, 265 (2018).
- [35] J. Zhang, G. Pagano, P. W. Hess, A. Kyprianidis, P. Becker, H. Kaplan, A. V. Gorshkov, Z.-X. Gong, and C. Monroe, *Nature (London)* **551**, 601 (2017).
- [36] X.-Y. Guo, C. Yang, Y. Zeng, Y. Peng, H.-K. Li, H. Deng, Y.-R. Jin, S. Chen, D. Zheng, and H. Fan, *Phys. Rev. Appl.* **11**, 044080 (2019).
- [37] T. Tian, H.-X. Yang, L.-Y. Qiu, H.-Y. Liang, Y.-B. Yang, Y. Xu, and L.-M. Duan, *Phys. Rev. Lett.* **124**, 043001 (2020).
- [38] P. Jurcevic, H. Shen, P. Hauke, C. Maier, T. Brydges, C. Hempel, B. P. Lanyon, M. Heyl, R. Blatt, and C. F. Roos, *Phys. Rev. Lett.* **119**, 080501 (2017).
- [39] E. A. Yuzbashyan, O. Tsypliyatyev, and B. L. Altshuler, *Phys. Rev. Lett.* **96**, 097005 (2006).
- [40] B. Sciolla and G. Biroli, *Phys. Rev. Lett.* **105**, 220401 (2010).
- [41] J. C. Halimeh, V. Zauner-Stauber, I. P. McCulloch, I. de Vega, U. Schollwöck, and M. Kastner, *Phys. Rev. B* **95**, 024302 (2017).
- [42] J. Marino, M. Eckstein, M. S. Foster, and A. M. Rey, *Rep. Prog. Phys.* **85**, 116001 (2022).
- [43] S. Vajna and B. Dóra, *Phys. Rev. B* **89**, 161105(R) (2014).
- [44] J. Yu, *Phys. Rev. A* **96**, 023601 (2017).

- [45] X. Qiu, T.-S. Deng, G.-C. Guo, and W. Yi, *Phys. Rev. A* **98**, 021601(R) (2018).
- [46] A. Lahiri and S. Bera, *Phys. Rev. B* **99**, 174311 (2019).
- [47] K. Sim, R. Chitra, and P. Mognini, *Phys. Rev. B* **106**, 224302 (2022).
- [48] M. Tarnowski, F. N. Ünäl, N. Fläschner, B. S. Rem, A. Eckardt, K. Sengstock, and C. Weitenberg, *Nat. Commun.* **10**, 1728 (2019).
- [49] H. Weyl, *Z. Phys.* **56**, 330 (1929).
- [50] P. Delpace, J. Li, and D. Carpentier, *Europhys. Lett.* **97**, 67004 (2012).
- [51] S.-Y. Xu, I. Belopolski, N. Alidoust, M. Neupane, G. Bian, C. Zhang, R. Sankar, G. Chang, Z. Yuan, C.-C. Lee *et al.*, *Science* **349**, 613 (2015).
- [52] C.-Z. Chen, J. Song, H. Jiang, Q. F. Sun, Z. Wang, and X. C. Xie, *Phys. Rev. Lett.* **115**, 246603 (2015).
- [53] N. P. Armitage, E. J. Mele, and A. Vishwanath, *Rev. Mod. Phys.* **90**, 015001 (2018).
- [54] Z.-Y. Wang, X.-C. Cheng, B.-Z. Wang, J.-Y. Zhang, Y.-H. Lu, C.-R. Yi, S. Niu, Y. Deng, X.-J. Liu, S. Chen *et al.*, *Science* **372**, 271 (2021).
- [55] See Supplemental Material at <http://link.aps.org/supplemental/10.1103/PhysRevB.109.L140303> for more examples of vortex loop dynamics for different 3D lattice models.
- [56] See Supplemental Material at <http://link.aps.org/supplemental/10.1103/PhysRevB.109.L140303> for a brief summary of notation conventions for fermionic operators used in this manuscript.
- [57] See Supplemental Material at <http://link.aps.org/supplemental/10.1103/PhysRevB.109.L140303> for a discussion on eigenstates of $H_{\mathbf{k}}$.
- [58] M. E. Peskin, *An Introduction to Quantum Field Theory* (CRC Press, Boca Raton, FL, 2018).
- [59] See Supplemental Material at <http://link.aps.org/supplemental/10.1103/PhysRevB.109.L140303> for a more detailed discussion of the Weyl Hamiltonian, its eigenenergies, Weyl nodes, and the quenches within the model.
- [60] See Supplemental Material at <http://link.aps.org/supplemental/10.1103/PhysRevB.109.L140303> for a calculation demonstrating the connection between the Green's function and the first-order correlation function.
- [61] T. V. Zache, N. Mueller, J. T. Schneider, F. Jendrzejewski, J. Berges, and P. Hauke, *Phys. Rev. Lett.* **122**, 050403 (2019).
- [62] The assumptions that \mathcal{M} and $\mathcal{M}_n(t)$ are 2D smooth surfaces is well justified as long as the Hamiltonian before and after the quench is described by smooth functions $\tilde{h}_{\mathbf{k}}^{(i)}$ and $\tilde{h}_{\mathbf{k}}^{(f)}$, which are also bounded as the lattice Hamiltonian $H_{\mathbf{k}}$ has a bounded spectrum, both from below and above.
- [63] This assumption is made under the condition that there are no surface parts touching, which represents a finely tuned scenario, for example, where $\mathcal{M} : f_1(k_x) = 0$ and $\epsilon_{\mathbf{k}} = f_2(k_x, t)$, which reduces to the 1D problem.
- [64] F. Hirzebruch, *Topological Methods in Algebraic Geometry* (Springer, Berlin, Heidelberg, 1966).
- [65] W. Magnus, *Commun. Pure Appl. Math.* **7**, 649 (1954).
- [66] S. Blanes, F. Casas, J. Oteo, and J. Ros, *Phys. Rep.* **470**, 151 (2009).
- [67] J. N. Kriel, C. Karrasch, and S. Kehrein, *Phys. Rev. B* **90**, 125106 (2014).
- [68] See Supplemental Material at <http://link.aps.org/supplemental/10.1103/PhysRevB.109.L140303> for a calculation of the evolution operator and correlation functions in the interacting case.
- [69] A. Kosior1 and M. Heyl, Vortex loop dynamics and dynamical quantum phase transitions in 3D fermion matter (2024), <https://doi.org/10.5281/zenodo.10837585>.